

A pressure-amplifying framework material with negative gas adsorption transitions

Simon Krause, Volodymyr Bon, Irena Senkovska, Ulrich Stoeck, Dirk Wallacher, Daniel M Többens, Stefan Zander, Renjith Pillai, Guillaume Maurin, François-Xavier Coudert, et al.

▶ **To cite this version:**

Simon Krause, Volodymyr Bon, Irena Senkovska, Ulrich Stoeck, Dirk Wallacher, et al.. A pressure-amplifying framework material with negative gas adsorption transitions. Nature, 2016, 532 (7599), pp.348-352. 10.1038/nature17430 . hal-02118754

HAL Id: hal-02118754
https://hal.science/hal-02118754

Submitted on 3 May 2019

HAL is a multi-disciplinary open access archive for the deposit and dissemination of scientific research documents, whether they are published or not. The documents may come from teaching and research institutions in France or abroad, or from public or private research centers.

L'archive ouverte pluridisciplinaire **HAL**, est destinée au dépôt et à la diffusion de documents scientifiques de niveau recherche, publiés ou non, émanant des établissements d'enseignement et de recherche français ou étrangers, des laboratoires publics ou privés.

A pressure amplifying framework material with negative gas adsorption transitions

Simon Krause, Volodymyr Bon, Irena Senkovska, Ulrich Stoeck, Dirk Wallacher, Daniel M. Többens, Stefan Zander, Renjith S. Pillai, Guillaume Maurin, François-Xavier Coudert & Stefan Kaskel

Adsorption-based phenomena play a key role in gas separations[1,2], including greenhouse[3] and toxic[4] gas pollutants treatment, and in water adsorption based heat pumps[5] for solar cooling systems. The ability to tune the pore size, shape and functionality of crystalline porous coordination polymers, or metal-organic frameworks (MOFs) has made them attractive materials for such sorption-based applications[3,6-8]. A unique feature of soft porous frameworks is their flexibility and guest dependent response[9,10] causing unexpected adsorption phenomena with attractive advantages for such sorption-based applications[11-14]. Common to all isothermal gas adsorption phenomena, however, is increased gas uptake with increased pressure. Here we report a new phenomenon of adsorption transitions in isotherms of a MOF, which exhibits a negative gas adsorption (NGA) - a point at which spontaneous desorption of gas occurs during pressure increase in a defined temperature and pressure range. Parallelized in situ powder X-ray diffraction (PXRD), gas adsorption experiments and simulations show that this adsorption behaviour is controlled by a guest-assisted hysteretic structural transition of the MOF. We anticipate our findings to be the basis for new technologies using NGA-capable frameworks for pressure amplification in micro- and macroscopic system engineering. NGA extends the series of counterintuitive phenomena such as negative thermal expansion[15,16], negative refractive indexes[17] and may be interpreted as an adsorptive analogue of force amplifying negative compressibility transitions proposed for metamaterials[18].

In MOFs, novel guest-assisted phenomena, such as ligand flip[19], gating[20], and breathing[21,22] of the framework lead to adsorption isotherms with S-shape, wide hysteresis and multiple steps[23], which give rise to new, previously unattainable potential applications[10]. As a rule of thermodynamics, at constant temperature the absolute amount of substance in the adsorbed phase (n_{ads}) always increases with increasing pressure of the adsorptive (p), resulting in a positive slope (1) in a single component adsorption isotherm (Fig. 1a)[24].

$$(dn_{ads}/dp) \geq 0 \quad (1)$$

In the following we describe a material with a paradoxical negative adsorption step causing an unexpected pressure amplification triggered by a unique structural transition of a nanoporous framework. We show that this novel phenomenon is observed upon adsorption of various gas molecules at characteristic temperature and pressure in DUT-49, a framework with very high porosity. Initially, DUT-49 was discovered as a high performance methane storage material for natural gas vehicles[25]. The extremely high excess methane storage capacity of 308 g kg^{-1} at 110 bar and 298 K motivated us to elucidate the adsorption mechanism at lower temperatures. However, a methane adsorption isotherm recorded at 111 K revealed a peculiar drop that was originally regarded as an instrumental failure (Fig. 1b). Repeated isotherm measurements at 111 K gave

evidence of a perfectly reproducible negative adsorption step around 10 kPa, strongly deviating from the previously reported adsorption profile at 298 K (up to 110 bar). With a drop of Δn_{NGA} = -8.62 mmol g^{-1} the NGA-step alone surpasses the adsorption capacity of commercially available nanoparticles and even of some zeolites[26]. Thus it is by no means negligible in volumetric adsorption experiments and causes a massive response and pressure amplification of Δp_{NGA}=2.27 kPa in the measuring cell (Fig. 1f) in stark contrast to any rigid microporous solids (Fig. 1e). This corresponds to a specific Δp_{NGA} for methane adsorption at 111 K of up to 493 kPa g^{-1} (Supplementary Tab. S1).

Additional adsorption experiments using *n*-butane at 298 K lead to a distinct NGA step at 30 kPa (Fig. 1c) with a kinetic profile (Fig. 1g) similar to that of methane (111 K) while isotherms of N_2 at 77 K (Supplementary Fig. S5) show a typical type I slope illustrating the subtle and specific impact of guest interaction on NGA in DUT-49. Gravimetric adsorption experiments with *n*-butane at 298 K in parallel to DSC support the results obtained from volumetric adsorption experiments and additionally reveal a combination of exothermic and endothermic processes during NGA substantiating the unique and complex mechanism of the transformation (Fig. 1d, Supplementary Fig. S24). Exposing samples of DUT-49 to *n*-butane is in particular illustrative since NGA can be explored at room temperature below 100 kPa corresponding to conditions easily attained in a standard laboratory environment. Visual monitoring of the sample during the adsorption experiment reveals macroscopic movement of the particle ensemble caused by the massive gas release during NGA, followed by a pronounced shrinkage of the packed bed volume by ca. 20 % (Fig. 1h, supplementary video 1). Based on this macroscopic observation we suspected NGA to be related to massive structural transformations in the crystalline solid. Real time parallelized adsorption/diffraction/EXAFS experiments carried out at the BESSY II light source at HZB (Berlin) using an improved setup[27] allowed us to elucidate the structural transformations *in situ*.

Synchrotron PXRD data collected during methane adsorption at 111 K indicate two distinct structural transitions of DUT-49*op* at 10 kPa and 45-65 kPa correlating to the steps in the isotherm (Fig. 2a and 2b). DUT-49*op* is an assembly of cuboctahedral metal-organic polyhedra (MOPs) formed by Cu_2-paddle-wheel units and 9*H*-carbazole-3,6-dicarboxylates connected by biphenylene units forming an **fcu** topology[25]. Wide open voids (1.0, 1.7 and 2.4 nm) originate from an ordered arrangement of MOPs, an expanded analogue of a cubic close packing of atoms but with huge tetrahedral and octahedral voids (Fig. 3, a-c). During NGA the highly porous framework undergoes a colossal contraction of the unit cell from V = 100,072 $Å^3$ (ρ_{calc} = 0.287 $g{\cdot}cm^{-3}$) to a highly squeezed intermediate, DUT-49*cp* with a cell volume of only 47,282 $Å^3$ (ρ_{calc} = 0.661 $g{\cdot}cm^{-3}$) (Supplementary Fig. S34) corresponding to a unit cell change of more than 50,000 $Å^3$ (Fig. 2c). This initial transformation is reversible and as the pores are completely filled, expansion back to the original DUT-49*op* is observed (Supplementary Fig. S35).

From a structural point of view the contraction originates from concerted rotation of the MOPs along the three-fold axis running along [111], leading to a severe deformation of the ligand (Fig. 3e, supplementary video2). Yet, the connectivity of the framework is preserved during the transformation and the porosity of the MOPs (d_{Pore} = 10.1 to 9.9 Å) is only slightly affected. EXAFS spectra collected *in situ* during methane adsorption at

111 K confirm the unaltered coordination environment of Cu^{2+} (Supplementary Figs. S38-39, Tab. S8). In contrast, the pore diameter of the tetrahedral voids is strongly reduced from 16.9 to 10.6 Å and the mesoporous octahedral voids deform even more drastically from 23.9 to 7.8 Å, resulting in a massive overall pore volume reduction by 61 % (see also visualization in supplementary video 2).

During desorption of methane at 111 K two gradual phase transitions from DUT-49*op* to DUT-49*ip* (V = 94457 $Å^3$, a = 45.54 Å, ρ = 0.332 $g \cdot cm^{-3}$) in the pressure range from 30 - 20 kPa and to DUT-49*cp* at pressures lower than 20 kPa were observed, resulting in a wide hysteresis. Remarkably, during desorption at 111 K the framework does not switch back to the open form even at very low pressures (Supplementary Fig. S6). However, transformation into DUT-49*op* can be achieved by heating at a constant methane pressure of 100 kPa from 111 K to 298 K followed by evacuation (Supplementary Fig. S7, S9). *In situ* PXRD/adsorption experiments of *n*-butane at 298K show similar DUT-49*op* - DUT-49*cp* transitions as observed for methane adsorption at 111 K (Supplementary Fig. S32).

Grand Canonical Monte Carlo simulations performed for methane at 111 K in both DUT-49*op* and DUT-49*cp* shed light on the microscopic adsorption mechanism in play. The experimental adsorption isotherm is precisely reproduced by simulating two adsorption regimes, starting with pore filling of DUT-49*op* up to 10 kPa, but continued adsorption in the contracted DUT-49*cp* (Fig. 4b, analogous observation for *n*-butane at 298 K; Supplementary Fig. S41). Methane occupies the smaller MOP cavities before gradually travelling over the tetrahedral and octahedral cages of DUT-49*op* with increasing pressure to attain a complete exploration of the mesopores at 11 kPa (Fig. 4c). Indeed, this scenario strongly suggests that the filling of the mesopores triggers the structure contraction responsible for NGA.

Further analysis by quantum chemistry calculations at Density Functional Theory (DFT) level showed that guest free DUT-49*cp* is energetically significantly destabilized (ΔE = 91 kJ mol^{-1} per linker molecule) as compared to DUT-49*op* due to the highly strained organic ligand (Fig. 3a,e). Upon adsorption, this energy difference is overcome by the higher affinity of methane for the contracted-pore structure due to the much smaller pores with deeper energy well of DUT-49*cp*. Given the adsorption enthalpies of DUT-49*cp* and DUT-49*op* (ΔH_{ads} ≈ 17 kJ mol^{-1} and 10 kJ mol^{-1} respectively) (Supplementary Fig. S44, Tab. S13), the difference in adsorption enthalpy in the transition region, ΔN_{ads} x $\Delta\Delta H_{ads}$ ≈ 130 kJ mol^{-1}, is in magnitude comparable to ΔE, explaining why adsorption compensates the energy penalty of the structural transition (Supplementary Tab. S15). Analysis of the elastic properties of DUT-49*op* completes this picture: While the bulk modulus of 8.7 GPa is in the usual range for metal-organic frameworks[29], the minimal shear modulus of the structure is relatively low at 1.5 GPa, with a strong nonlinearity showing a soft deformation mode that can be triggered by adsorption.

Summarizing, in NGA a highly overloaded metastable state is created by adsorption in a hierarchical pore structure which is spontaneously released when the energy barrier is overcome. Reduction of porosity through network deformation triggered by adsorption-induced stress and subsequent release of previously adsorbed gas is the result. Extended equilibration times up to several hours (Supplementary Fig. S14) refute that this

phenomenon is caused by inadequate equilibration of the system but indicate the presence of long-lived metastable states, possibly due to the vast extent of deformation and crossover of pore sizes (Fig. 3d), compared with prominent purely microporous breathing systems such as MIL-53[21]. This implies internal reshuffling of molecules in DUT-49 from rigid MOP pores into contracted octahedral voids. Along these lines is also the temperature dependence of NGA: Adsorption of methane at 91, 111, 101, and 121 K (Fig. 4a, d) and *n*-butane at 273 - 308 K (Supplementary Fig. S10) suggest even a slight $|\Delta n_{NGA}|$ increase with temperature up to 9.87 mmol(CH_4) g^{-1} at 121 K while the pore contraction mechanism and relative pressure (p/p_0 = 0.1-0.15) responsible for NGA is retained (Supplementary Fig. S27, S30) clearly supporting that filling of the mesopores induces the contraction (Fig. 4a,c).

To our knowledge, pressure amplifying materials of this magnitude have never been reported before. Metastable cation complexes in zeolite materials could be considered as a rare analogue[30]. Beyond the fundamental fascination of this new phenomenon, implications for technological applications cannot be emphasized strongly enough. Conceptually, these new materials contain all required features for the design of threshold sensitive micropneumatic devices, or stimuli responsive self-propelling systems. In this respect, negative gas adsorption frameworks may be useful as mechanical actuators responding selectively towards changes in the environment, capable to transform a high amount of latent strain into pressure. This phenomenon is certainly unique and novel in the field of porous solids.

References

1 de Vos, R. M. & Verweij, H. High-selectivity, high-flux silica membranes for gas separation. *Science* **279**, 1710-1711, doi:10.1126/science.279.5357.1710 (1998).

2 Nenoff, T. M. Hydrogen purification: MOF membranes put to the test. *Nat. Chem* **7**, 377-378, doi:10.1038/nchem.2218 (2015).

3 McDonald, T. M. *et al.* Cooperative insertion of CO_2 in diamine-appended metal-organic frameworks. *Nature* **519**, 303-308, doi:10.1038/nature14327 (2015).

4 Barea, E., Montoro, C. & Navarro, J. A. R. Toxic gas removal - metal-organic frameworks for the capture and degradation of toxic gases and vapours. *Chem. Soc. Rev.* **43**, 5419-5430, doi:10.1039/c3cs60475f (2014).

5 Furukawa, H. *et al.* Water adsorption in porous metal–organic frameworks and related materials. *J. Am. Chem. Soc.* **136**, 4369-4381, doi:10.1021/ja500330a (2014).

6 Kitagawa, S., Kitaura, R. & Noro, S.-i. Functional porous coordination polymers. *Angew. Chem. Int. Ed.* **43**, 2334-2375, doi:10.1002/anie.200300610 (2004).

7 Furukawa, H., Cordova, K. E., O'Keeffe, M. & Yaghi, O. M. The chemistry and applications of metal-organic frameworks. *Science* **341**, doi:10.1126/science.1230444 (2013).

8 Nugent, P. *et al.* Porous materials with optimal adsorption thermodynamics and kinetics for CO_2 separation. *Nature* **495**, 80-84, doi:10.1038/nature11893 (2013).

9 Horike, S., Shimomura, S. & Kitagawa, S. Soft porous crystals. *Nat Chem* **1**, 695-704, doi:10.1038/nchem.444 (2009).

10 Schneemann, A. *et al.* Flexible metal-organic frameworks. *Chem. Soc. Rev.* **43**, 6062-6096, doi:10.1039/c4cs00101j (2014).

11 Matsuda, R. Materials chemistry: Selectivity from flexibility. *Nature* **509**, 434-435, doi:10.1038/509434a (2014).

12 Sato, H. *et al.* Self-accelerating CO sorption in a soft nanoporous crystal. *Science* **343**, 167-170, doi:10.1126/science.1246423 (2014).

13 Takashima, Y. *et al.* Molecular decoding using luminescence from an entangled porous framework. *Nat. Commun.* **2**, 168, doi:10.1038/ncomms1170 (2011)

14 Yang, S. *et al.* A partially interpenetrated metal–organic framework for selective hysteretic sorption of carbon dioxide. *Nat. Mater.* **11**, 710-716, doi:10.1038/nmat3343 (2012).
15 Martinek, C. & Hummel, F. A. Linear thermal expansion of three tungstates. *J. Am. Ceram. Soc.* **51**, 227-228, doi:10.1111/j.1151-2916.1968.tb11881.x (1968).
16 Koshi, T. Negative thermal expansion materials: technological key for control of thermal expansion. *Sci. Tech. Adv. Mater.* **13**, 013001, doi:10.1088/1468-6996/13/1/013001 (2012).
17 Shelby, R. A., Smith, D. R. & Schultz, S. Experimental verification of a negative index of refraction. *Science* **292**, 77-79, doi:10.1126/science.1058847 (2001).
18 Nicolaou, Z. G. & Motter, A. E. Mechanical metamaterials with negative compressibility transitions. *Nat. Mater.* **11**, 608-613, doi:10.1038/nmat3331 (2012).
19 Fairen-Jimenez, D. *et al.* Opening the gate: Framework flexibility in ZIF-8 explored by experiments and simulations. *J. Am. Chem. Soc.* **133**, 8900-8902, doi:10.1021/ja202154j (2011).
20 Kondo, A. *et al.* Novel expansion/shrinkage modulation of 2D layered MOF triggered by clathrate formation with CO_2 molecules. *Nano Lett.* **6**, 2581-2584, doi:10.1021/nl062032b (2006).
21 Serre, C. *et al.* An explanation for the very large breathing effect of a metal–organic framework during CO2 adsorption. *Adv. Mater.* **19**, 2246-2251, doi:10.1002/adma.200602645 (2007).
22 Ferey, G. & Serre, C. Large breathing effects in three-dimensional porous hybrid matter: facts, analyses, rules and consequences. *Chem. Soc. Rev.* **38**, 1380-1399, doi:10.1039/b804302g (2009).
23 Salles, F. *et al.* Multistep N2 breathing in the metal−organic framework Co(1,4-benzenedipyrazolate). *J. Am. Chem. Soc.* **132**, 13782-13788, doi:10.1021/ja104357r (2010).
24 Thommes, M. *et al.* Physisorption of gases, with special reference to the evaluation of surface area and pore size distribution (IUPAC Technical Report). *Pure Appl. Chem.*, doi:10.1515/pac-2014-1117 (2015).
25 Stoeck, U., Krause, S., Bon, V., Senkovska, I. & Kaskel, S. A highly porous metal-organic framework, constructed from a cuboctahedral super-molecular building block, with exceptionally high methane uptake. *Chem. Commun.* **48**, 10841-10843, doi:10.1039/c2cc34840c (2012).
26 Traa, Y. & Weitkamp, J. in *Handbook of Porous Solids* 1015-1057 (Wiley-VCH Verlag GmbH, 2008).
27 Bon, V. *et al.* In situ monitoring of structural changes during the adsorption on flexible porous coordination polymers by X-ray powder diffraction: Instrumentation and experimental results. *Microporous Mesoporous Mater.* **188**, 190-195, doi:10.1016/j.micromeso.2013.12.024 (2014).
28 Neimark, A. V., Coudert, F.-X., Boutin, A. & Fuchs, A. H. Stress-Based Model for the Breathing of Metal−Organic Frameworks. *The Journal of Physical Chemistry Letters* **1**, 445-449, doi:10.1021/jz9003087 (2010).
29 Tan, J. C. & Cheetham, A. K. Mechanical properties of hybrid inorganic-organic framework materials: establishing fundamental structure-property relationships. *Chem. Soc. Rev.* **40**, 1059-1080, doi:10.1039/c0cs00163e (2011).
30 Riekert, L. Instability of sorption complexes in synthetic faujasites. *J. Phys. Chem.* **73**, 4384-4386, doi:10.1021/j100846a066 (1969).

Figure 1 | **Gas adsorption isotherms, pressure and kinetic profiles**. **a,** Typical profile of type I adsorption isotherms for a non-breathing microporous solid and corresponding dn/dp[24]. **b, c,** adsorption isotherms (blue) and corresponding derivatives (red) of DUT-49 for methane at 111 K (**b**) and butane at 298 K (**c**). Δn_{NGA} represents the NGA-step in the isotherm. **d**, Gravimetric adsorption in parallel to dynamic scanning calorimetry (DSC), Δm_{NGA} represents the mass of the gas, released during NGA. **e, f, g,** Corresponding kinetic pressure profiles for typical adsorption behavior of a non-breathing microporous solid (**e**) and observed during the NGA-step for methane at 111 K (**f**) and *n*-butane at 298 K (**g**), gray areas indicate the dosing interval. **h,** Snapshots of video (Supplementary video 1) recorded during the *n*-butane adsorption steps at 298 K (**c, g**) (the capillary diameter is 1 mm and the sample bed 5 cm in height at t = 0s).

Figure 2 | ***In situ*** **powder X-ray diffraction (PXRD) during methane adsorption at 111 K. a**, Methane adsorption and desorption isotherms at 111 K collected *in situ*. The points corresponding to collected PXRD patterns are represented as solid symbols. **b**, Contour plot of the PXRD pattern evolution during adsorption (blue) and desorption (red). (*op* = open pore phase (cubic, *F*23, *a* = 46.427(4) Å), *cp* = contracted pore phase (cubic, $Pa\bar{3}$, *a* = 36.1603(2) Å), *ip* = intermediate pore phase (cubic, $Pa\bar{3}$, *a* = 45.542(2) Å)). **c**, Lattice parameter evolution during adsorption and desorption.

Figure 3 | **Structure of DUT-49*op* and DUT-49*cp***. **a**, **e**, Conformation of 9,9'-([1,1'-biphenyl]-4,4'-diyl)bis(9*H*-carbazole-3,6-dicarboxylate) in DUT-49op (**a**) and DUT-49cp (**e**). **b**, View of the crystal structure along [110] for DUT-49*op* (simulated accessible surface area 5049 $m^2 \cdot g^{-1}$, free pore volume 2.94 $cm^3\ g^{-1}$) (**b**) and DUT-49*cp* (simulated accessible surface area 2908 $m^2\ g^{-1}$, free pore volume 1.13 $cm^3 g^{-1}$) (**f**), color code for the atoms: C (dark grey), N (blue), O (red), Cu (cyan), H (light grey). Guest molecules are omitted for clarity. **c**,**g**, Pore representation of DUT-49*op* (**c**) and DUT-49*cp* (**g**) along [110] as natural tilings of **nbo** net. Color code for pore representation: cuboctahedral MOP cavity (green), tetrahedral cavity (yellow), octahedral cavity (orange). **d**, Evolution of pore sizes and free pore volume during contraction from DUT-49*op* to DUT-49*cp* and **h**, Evolution of density and accessible geometric surface area. Details about the simulation of intermediate structures, free pore volume, accessible surface area and pore sizes are given in Fig. S40.

Figure 4 | **Temperature dependent methane adsorption and simulations. a**, **d**, Methane adsorption isotherms at different temperatures. **b**, Experimental (gray) and simulated methane sorption isotherm at 111 K based on the crystal structures of DUT-49*op* (red) and DUT-49*cp (blue)*. **c**, Maps of the occupied positions of methane (green) in 1000 equilibrated frames for a given pressure for DUT-49*op* and at the transition pressure (11 kPa) of DUT-49*cp* (bottom frame), color code for the atoms: C (dark grey), N (blue), O (red), Cu (cyan), H (light grey). **e**, Schematic representation of stress-based model for adsorption-induced structural transformation[28], equilibrium transition (gray line), metastable transition (black arrows), open-pore phase (red line), contracted-pore phase (blue line), arrows indicate the transition observed for DUT-49.

Acknowledgements:

V.B. thanks the German Federal Ministry for education and research (Project BMBF No 05K13OD3). S.Kr., V.B., I.S. and S.Ka. thank HZB for financial support and allocation of synchrotron radiation beamtime at KMC-2 beamline. F.-X.C. acknowledges the access to HPC resources from GENCI (grant No. x2015087069). Authors thank Ulrike Koch for SEM images as well as Lev Sarkisov and Alain Fuchs for helpful discussions.

These authors contributed equally to this work: Simon Krause & Volodymyr Bon

Author Contributions: S. Kr. and U. S. synthesized and activated the investigated material; S. Kr., V. B., I. S. and S. Ka. conducted and interpreted volumetric and gravimetric sorption experiments; S. Kr, V. B., D. W. and D. M. T. conducted the *in situ* PXRD investigations, S. Kr, V. B., D. W. and S. Z. conducted the *in situ* EXAFS investigations; V. B. performed crystal structure solution and structure modeling; S. Kr. performed filming and animation of the structural transitions; F. X. C. performed quantum mechanical calculations; G. M. and R. S. P. performed Grand Canonical Monte Carlo simulations of adsorption; S. Kr., V.B., I. S., F. X. C. S., G. M. and S. Ka. wrote the manuscript.

Author Information: Crystal structures of DUT-49*op* in vacuum at 111 K, DUT-49*cp*⊃432CH_4 (number of methane molecules per unit cell) at 0.28 relative pressure of methane at 111 K during adsorption, DUT-49*op*⊃1344CH_4 at 0.97 relative pressure of methane at 111 K during adsorption, DUT-49*ip*⊃1176CH_4 at 0.25 relative pressure of methane at 111 K during desorption are available free of charge from the Cambridge Crystallographic Data Centre www.ccdc.cam.ac.uk/data_request/cif under reference numbers CCDC-1413081, CCDC-1413083, CCDC-1413082 and CCDC-1413084, respectively. Reprints and permissions information is available at www.nature.com/reprints. The authors declare no competing financial interests. Readers are welcome to comment on the online version of the paper. Correspondence and requests for materials should be addressed to Stefan Kaskel (stefan.kaskel@chemie.tu-dresden.de).

Affiliations:

Department of Inorganic Chemistry, Technische Universität Dresden, Bergstr. 66, 01062 Dresden, Germany.

Simon Krause, Volodymyr Bon, Irena Senkovska, Stefan Kaskel, Ulrich Stoeck (current affiliation: Institute for Complex Materials, Leibniz Institute for Solid State and Materials Research (IFW) Dresden, Helmholtzstraße 20, D-01069 Dresden, Germany.

PSL Research University, Chimie ParisTech – CNRS, Institut de Recherche de Chimie Paris, 75005 Paris, France.

François-Xavier Coudert

Institut Charles Gerhardt Montpellier UMR 5253 CNRS UM ENSCM, Université Montpellier, Place E. Bataillon, 34095 Montpellier cedex 05, France.

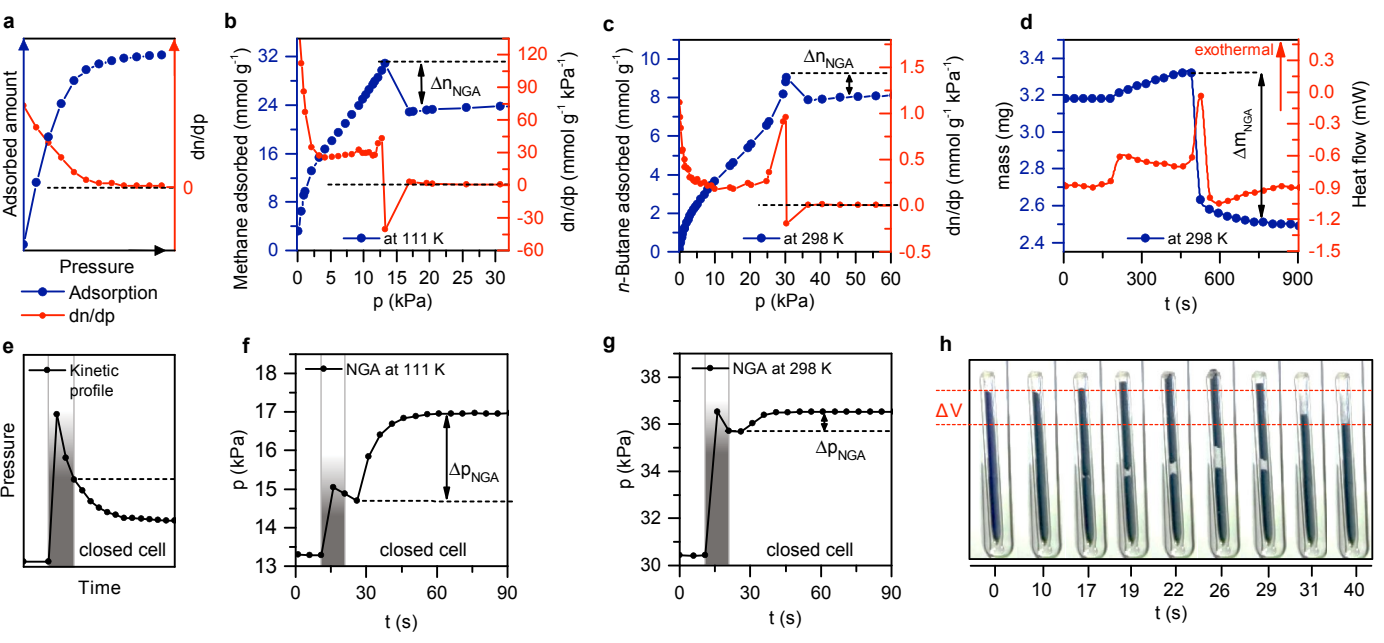
Renjith S. Pillai, Guillaume Maurin

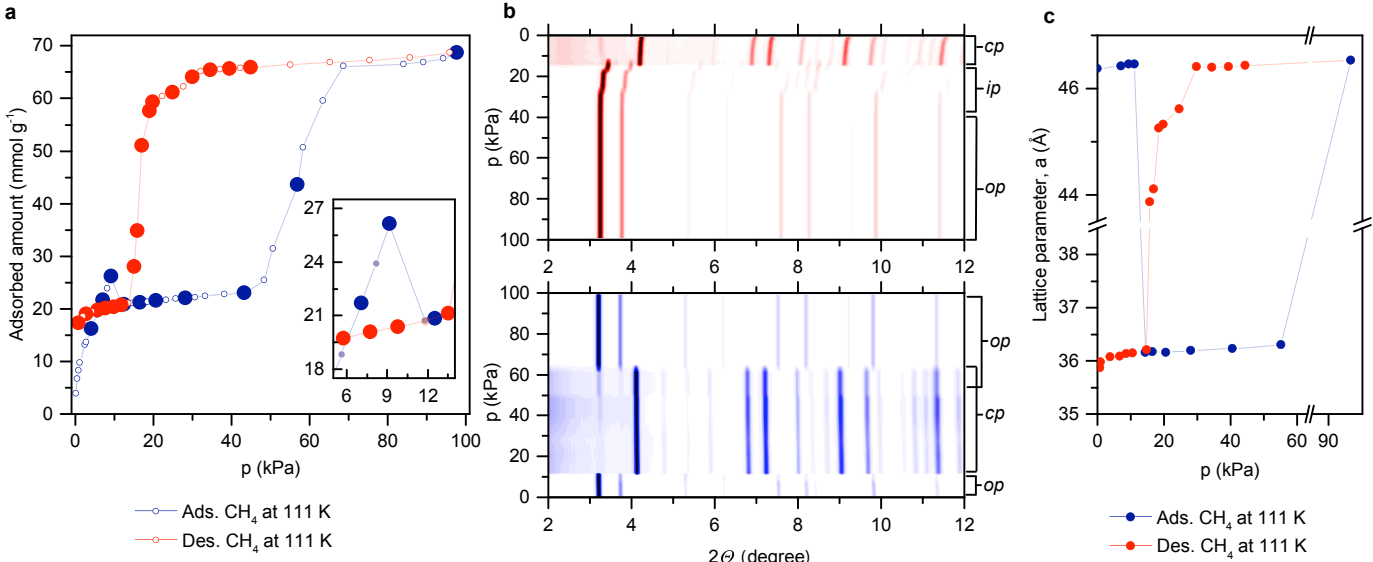
Department Sample Environments, Helmholtz-Zentrum Berlin für Materialien und Energie, Hahn-Meitner-Platz 1, 14109 Berlin, Germany.

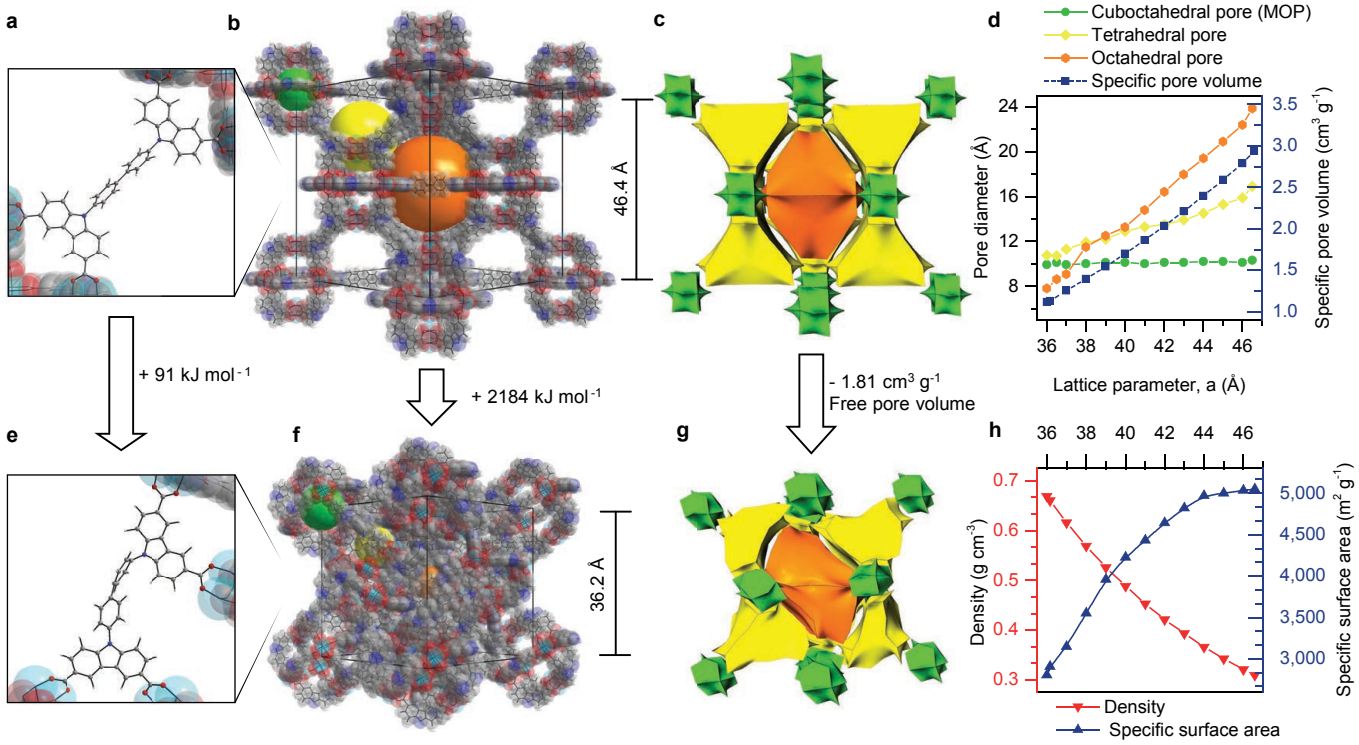
Dirk Wallacher

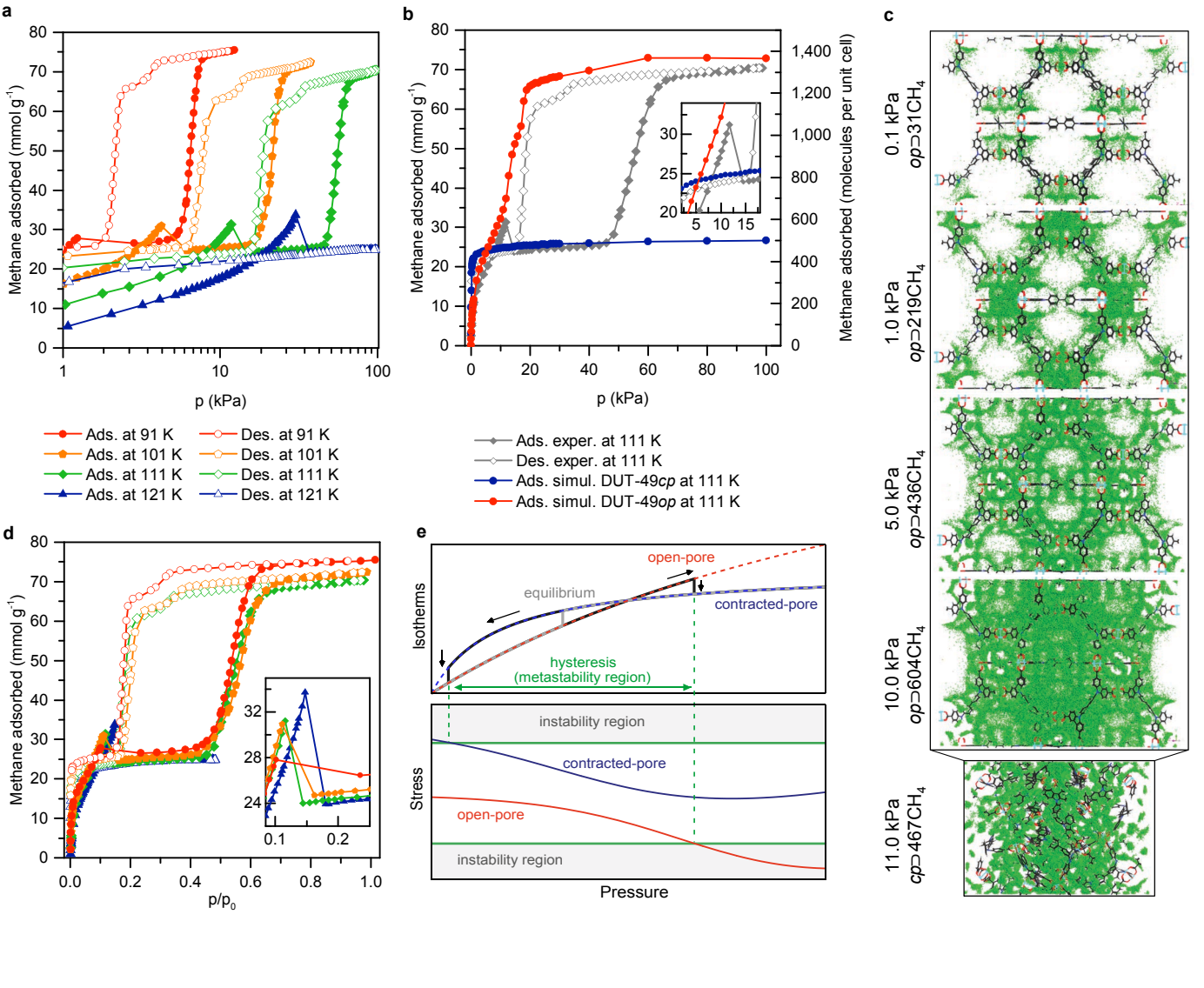
Department of Structure and Dynamics of Energy Materials, Hahn-Meitner-Platz 1, 14109 Berlin, Germany.

Daniel M. Többens, Stefan Zander


a
Adsorbed amount
dn/dp
Pressure
Adsorption
dn/dp
b
Methane adsorbed (mmol g-1)
dn/dp (mmol g-1 kPa-1)
Δn_NGA
at 111 K
p (kPa)
c
n-Butane adsorbed (mmol g-1)
dn/dp (mmol g-1 kPa-1)
Δn_NGA
at 298 K
p (kPa)
d
mass (mg)
Heat flow (mW)
exothermal
Δm_NGA
at 298 K
t (s)
e
Kinetic profile
Pressure
closed cell
Time
f
NGA at 111 K
p (kPa)
Δp_NGA
closed cell
t (s)
g
NGA at 298 K
p (kPa)
Δp_NGA
closed cell
t (s)
h
ΔV
t (s)


a
Adsorbed amount (mmol g-1)
p (kPa)
Ads. CH4 at 111 K
Des. CH4 at 111 K
b
p (kPa)
cp
ip
op
2Θ (degree)
c
Lattice parameter, a (Å)
p (kPa)
Ads. CH4 at 111 K
Des. CH4 at 111 K


a
b
c
d
e
f
g
h
46.4 Å
36.2 Å
+ 91 kJ mol-1
+ 2184 kJ mol-1
- 1.81 cm3 g-1
Free pore volume
Cuboctahedral pore (MOP)
Tetrahedral pore
Octahedral pore
Specific pore volume
Pore diameter (Å)
Specific pore volume (cm3 g-1)
Lattice parameter, a (Å)
Density (g cm-3)
Specific surface area (m2 g-1)
Density
Specific surface area


a
Methane adsorbed (mmol g-1)
p (kPa)
Ads. at 91 K
Ads. at 101 K
Ads. at 111 K
Ads. at 121 K
Des. at 91 K
Des. at 101 K
Des. at 111 K
Des. at 121 K
b
Methane adsorbed (mmol g-1)
Methane adsorbed (molecules per unit cell)
p (kPa)
Ads. exper. at 111 K
Des. exper. at 111 K
Ads. simul. DUT-49cp at 111 K
Ads. simul. DUT-49op at 111 K
c
0.1 kPa
op⊃31CH4
1.0 kPa
op⊃219CH4
5.0 kPa
op⊃436CH4
10.0 kPa
op⊃604CH4
11.0 kPa
cp⊃467CH4
d
Methane adsorbed (mmol g-1)
p/p0
e
Isotherms
equilibrium
open-pore
contracted-pore
hysteresis
(metastability region)
Stress
instability region
contracted-pore
open-pore
instability region
Pressure